Biochemical Engineering Journal 168 (2021) 107933

Contents lists available at ScienceDirect

Biochemical Engineering Journal

journal homepage: www.elsevier.com/locate/bej

Quantification of the effects of hydrophobicity and mass loading on the effective coverage of surface-immobilized elastin-like peptides

Zihang Su [a], ChulOong Kim [b], Julie N. Renner [a,*]

[a] Department of Chemical and Biomolecular Engineering, Case Western Reserve University, Cleveland, OH, 44106, United States
[b] Department of Chemical and Biological Engineering, Colorado School of Mines, Golden, CO, 80401, United States

ARTICLE INFO

Keywords:
Elastin-like polypeptides
Electrode modification
Cyclic voltammetry
Biotechnology

ABSTRACT

Elastin-like peptides (ELPs) immobilized to solid surfaces have recently gained attention for use in electrochemical applications in sensing as well as bioenabled electrode assembly. Key to the success of these applications is understanding how ELPs impact the access and electron transfer of reacting species to the solid surface (effective surface coverage). In this study, short ELPs with varying hydrophobicity and sequence length were designed for gold attachment, and the effect on the ability of a redox probe to access a gold surface was characterized by cyclic voltammetry. A quantitative model describing the relationship between ELP effective surface coverage as a function of mean hydrophobicity and mass loading was elucidated based on the results, showing the ability to precisely control surface properties by tuning the ELP sequence. This model will be useful for the design of surface-bound ELP sequences that exhibit desired effective surface coverage for electrochemical as well as biomaterial applications.

1. Introduction

Recently, protein and polypeptide engineering have emerged as promising tools for electrochemical applications. Taking advantage of the ability to precisely define sequences and achieve multiple specific functions, protein and polypeptide-containing thin film electrode modifications have already been applied to biosensing, enzyme-based electrode design, and biomedical device manufacturing [1–3].

Elastin is a particularly attractive polypeptide platform for electrochemical applications. Engineered elastin-like polypeptide sequences (ELPs) are derived from the hydrophobic domains of tropoelastin, with a repetitive motif consisting of Val-Pro-Gly-Xaa-Gly, where X is a guest residue that can be substituted by any amino acid except proline [4]. ELPs are well-known as stimuli-responsive biopolymers, exhibiting reversible thermal-dependent lower solution critical temperature (LCST) behavior in aqueous solutions, where they are soluble below the transition temperature and insoluble above it. This transition temperature (T_t) is dependent on the environmental conditions [5,6] as well as peptide concentration, chain length [7], and hydrophobicity [8]. With these unique sequence-defined characteristics ELPs have been designed for variety of applications, such as: protein purification, drug delivery, and tissue engineering [9]. The transition behavior of ELPs is also maintained in immobilized assemblies, leading to surface-bound "smart" applications [10].

Label-free electrochemical sensing platforms based on ELP transducers assembled on gold surfaces have recently been explored, where it was observed that elastin in the collapsed state blocks electron transfer between a redox probe, specifically the common $Fe(CN)_6^{3-/4-}$ redox couple, and the gold electrode surface [11]. When the immobilized elastin was in the extended state, the redox probe could access the electrode surface and electron transfer happened more readily. In essence, the changes observed via electrochemical impedance spectroscopy were indicative how exposed the gold surface was to the electrolyte when modified with molecular layers. The integrity of immobilized lipid bilayers have been similarly analyzed using cyclic voltammetry [12]. However, the impact of changing the assembled ELP guest residue content and mass loading on surface exposure, as measured via electron transfer performance between a redox probe and the gold electrode, is largely unexplored. The sensitivity of elastin-based electrochemical sensing platforms depends on the differences in surface exposure, which may vary depending on the chosen ELP sequence. In addition, the application of ELPs has expanded to bioenabled electrode assembly, where surface access and chemical versatility is desired [13–17]. There has also been a particular recent interest in exploiting

* Corresponding author.
E-mail address: jxr484@case.edu (J.N. Renner).

https://doi.org/10.1016/j.bej.2021.107933
Received 17 August 2020; Received in revised form 3 December 2020; Accepted 21 December 2020
Available online 23 January 2021

the responsive behavior of short elastin polypeptides on functionalized gold nanoparticles [18], which is useful in other non-electrochemical areas including drug delivery [19], imaging [20], and as active plasmonic waveguides [21]. Surface exposure is also important in these applications, as exposed substrates may be prone to biofouling [22].

In this study, we hypothesize that surface access (or effective surface coverage), as measured via electron transfer between a redox probe and the gold electrode, can be controlled by modifying the guest residue hydrophobicity and mass loading of assembled engineered short ELPs. Herein, we utilized cyclic voltammetry (CV) to investigate the effective surface coverage of different ELPs when assembled on gold electrodes with varying guest residues and length. A quartz crystal microbalance with dissipation (QCM-D) was utilized to estimate the mass loading and observe the layer formation process. The results show that effective surface coverage can be precisely and predictably tuned using assembled ELPs. The proposed model for effective surface coverage will serve as guidance for future ELP-based electrochemical sensing platforms and electrode design.

2. Materials and methods

2.1. Materials

Detailed materials information is provided in the Supplementary Data.

2.2. Peptide design

Peptide sequences utilized in this study consisted of an elastin-like motif, $(VPGXG)_n$, where n = number of pentapeptide repeats. The N-terminus was modified with cysteine (C) for all peptides. The ends of the peptides were acylated and amidated. All sequences are shown in Table S1. All peptides were purchased from GenScript at purities above 95 %.

2.3. Electrode preparation

Screen printed electrodes (Metrohm DropSens, DRP-220BT, L33 × W10 × H0.5 mm) with a gold working electrode (4 mm diameter), sliver reference electrode, and platinum counter electrode were used in this study. Before electrode functionalization, all SPEs were prepared by cleaning in 0.5 M H_2SO_4 solution (60 μ L to fully cover the SPE electrodes), preforming cyclic voltammetry scans from -0.2 V to 1.3 V (versus internal silver reference electrode) at a scan rate of 100 mV s^{-1}, with 9 scan accumulations [23]. After cleaning, SPEs were rinsed with deionized (DI) water and dried with N_2. All SPEs were used once per test in this study, and not reused.

2.4. Peptide incubation

All peptides were prepared at 10 μg/mL in 0.01 M phosphate buffered saline (PBS, pH 7.4). For experiments on screen-printed electrodes, 60 μL of the peptide solution was deposited on the SPE electrode surface. The same amount of PBS solution (60 μL) was added for the bare electrode experiments. To ensure the electrode surface was maximally saturated with peptide adsorption, all SPE samples were incubated for overnight at 4℃. Prior to electrochemical characterization, electrodes were gently rinsed with PBS solution and dried with N_2 gas. All peptide solutions were prepared freshly prior to experiments. In buffer concentration experiments, all solutions were made in 0.1 M PBS (pH = 7.4) unless otherwise stated.

2.5. Cyclic voltammetry

All electrochemical experiments were performed on SPEs that connected to a Metrohm Autolab potentiostat (controlled by Nova 2.1 software). The redox buffer contained equimolar amounts of 4 mM $K_3Fe(CN)_6$ and 4 mM $K_4Fe(CN)_6$ in 0.01 M PBS (pH 7.4) with 0.1 M KCl. Cyclic voltammetry (CV) measurements on SPEs were conducted at room temperature, at a range of -0.2 V to 0.6 V and a scan rate of 100 mV s^{-1} without any preconditional potential or accumulation time. For each sample, 60 μL redox solution was used to fully cover the SPE electrodes, and five scans were collected. In forward of CV scans, ferrocyanide is oxidized to ferricyanide, and in reverse scans, ferricyanide is reduced to ferrocyanide. Experiments with varying scan rate were collected using equimolar amounts of 5 mM $K_3Fe(CN)_6$ and 5 mM $K_4Fe(CN)_6$ in 0.01 M PBS (pH 7.4) with 0.1 M KCl at a range of 10-100 mV s^{-1}. Redox probe concentration experiments were collected with equimolar solutions from 0 to 100 mM in 0.01 M PBS with 0.1 M KCl solution at 50 mV s^{-1}.

2.6. Quartz crystal microbalance with dissipation

A quartz crystal microbalance with dissipation (QCM-D, QSense Explorer, controlled by QSoft software, Biolin Scientific) was used to investigate the peptide adsorption behavior and the relative mass loading of each peptide on gold surfaces. Frequency shifts and dissipation changes were monitored simultaneously versus time. The details of these experiments can be found in our previous work [15,16], and in the Supplementary Data.

2.7. Circular dichroism

Circular dichroism (CD) spectroscopy was utilized to analyze the secondary structure of triple-repeat elastin-like peptides. Procedures can be found in our previous work [16], with details in the Supplementary Data.

2.8. Atomic force microscopy

Atomic force microscopy (AFM) was used to analyze the topography of surface-immobilized triple-repeat elastin-like peptides VKV and KVK. Procedures can be found in our previous work [15,16], with details in the Supplementary Data.

2.9. Statistical analysis

Data are represented as the mean ± the standard deviation. Analysis of variance (ANOVA) was performed using Minitab to determine if a factor had a significant effect. Statistical groupings were determined by Tukey's *post hoc* test. Simple linear regression of average values was performed using Minitab. Best fit lines were obtained using the method of least squares. All statistical tests used $\alpha = 0.05$. For results in the main text, n = 3 except in the case of single-repeated peptide where X = E (n = 5) and triple-repeated peptide where $X = K_3$ (n = 4).

3. Results

3.1. The influence of gold-immobilized single-repeat ELP guest residue on $Fe(CN)_6^{3-/4-}$ electron transfer

Cyclic voltammetry (CV) was performed in the presence of a $Fe(CN)_6^{3-/4-}$ redox probe on gold electrodes with assembled ELPs. To investigate the effect of guest residue hydrophobicity, single-repeat elastin peptides with different guest residues were designed with the sequence Ac-CVPGXG-NH_2, featuring an N-terminal cysteine (C) for rapid immobilization to the gold surface via a thiol bond. Table S1 contains all sequences explored in this study. All peptides were acetylated and amidated to ensure any charge effects were imparted only by the guest residues. Lysine (K) and glutamic acid (E), served respectively as positively and negatively charged guest residues. Valine (V) and tyrosine (Y) were selected as neutral guest residues of varying

hydrophobicity. The single-repeat peptides were assembled on prepared screen printed electrodes (SPEs) and exposed to the redox solution. Each CV experiment consisted of five scans. Stable data indicated the assembled elastin did not change significantly during the scanning period (Fig. S1). Representative CVs are shown in Fig. 1.

On bare gold electrodes, as shown in Fig. 1 (black line), a pair of redox peaks was observed, with a peak-to-peak separation of ~60 mV which is expected for diffusion-controlled, reversible redox reactions. In contrast, CVs taken on peptide-modified electrodes either had no discernible peaks, or had increased peak-to-peak separations, which is indicative of a quasi-reversible redox reaction. Plots of peak current versus the square root of scan rate for selected peptides in this study (Fig. S2) confirm the quasi-reversible nature, with slight deviations from perfect linearity observed. In addition, the peak currents observed on peptide-modified electrodes were lower compared to peak currents observed on bare electrode. The results indicated that all ELPs were successfully immobilized on electrode surface, and different peptide layers were reducing the available electrode surface area or hindering the ability of electron transfer from the redox probe in solution to the underlying electrode.

To quantify the extent to which the peptides block electron transfer, the total charge passed on the second CV scan of each peptide sample was normalized to the bare gold electrode sample. Thus, to compare samples we define effective surface coverage, f_e, as:

$$f_e = 1 - \frac{\text{total charge for sample } (C_i)}{\text{total charge for bare gold } (C_0)} \quad (1)$$

Using this definition, we discovered f_e was guest residue dependent, being 0.24 ± 0.03, 0.38 ± 0.12, 0.43 ± 0.11, 0.57 ± 0.02 for guest residue X = K, E, Y and V, respectively. We observed that in general f_e was positively related to hydrophobicity, with immobilized peptides containing guest residue X = V, Y and E in one statistical grouping, and X = Y, K, E being in another statistical grouping (see Table S2 for ANOVA and *post hoc* testing results). V and K peptides had significantly different results, indicating that hydrophobicity of the guest residue has a significant impact on electron transfer.

3.2. The influence of gold-immobilized double- and triple-repeat ELP guest residue on $Fe(CN)_6^{3-/4-}$ electron transfer

To further investigate the effects of ELP guest residue hydrophobicity

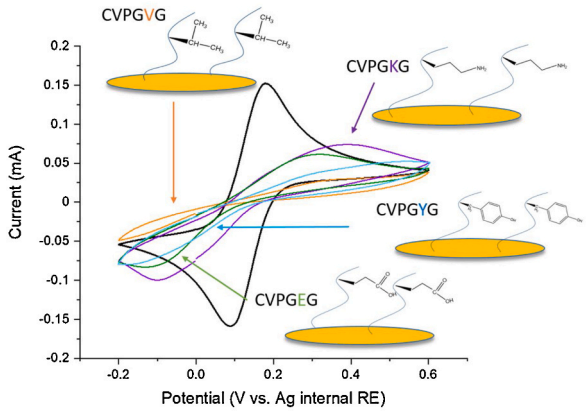

Fig. 1. Cyclic voltammograms obtained on ELP-modified SPEs with varying ELP guest residue hydrophobicity demonstrate controlled electron transfer of a label-free redox probe. Results were collected in 0.01 M PBS with 4 mM Fe $(CN)_6^{3-/4-}$ redox couple and 0.1 M KCl, from -0.2 V to 0.6 V (vs. sliver internal reference electrode) with a 0.1 V/s scan rate. Representative data are shown, and include bare gold SPE electrode (black), V peptide modified electrode (orange), K peptide modified electrode (purple), E peptide modified electrode (green), and Y peptide modified electrode (blue).

and length in controlling f_e, double- and triple-repeat ELPs were designed with varying ratios of positively charged guest residue (K) and neutral hydrophobic guest residue (V) (Table S1 contains exact peptide sequences). Briefly, three double-repeat peptides were designed having the general form of Ac-CVPGX$_1$GVPGX$_2$G-NH$_2$, with guest residues occurring in the order X_1X_2 = K_2, VK and V_2. Three triple-repeat peptides were designed with the general form of Ac-CVPGX$_1$GVPGX$_2$GVPGX$_3$G-NH$_2$, with guest residues occurring in the order $X_1X_2X_3$ = K_3, KVK and VKV. Fig. 2 shows the representative CV scans on double- and triple- repeat peptide functionalized electrodes as well as a bare gold electrode for comparison.

The CVs obtained on electrodes functionalized with double- and triple-repeat ELPs exhibited a similar trend shown in Fig. 1, where it was observed that as the fraction of V increases, the average hydrophobicity increases, and f_e increases, coinciding with an increase in peak-to-peak separation and decrease in peak current. For electrodes functionalized with double-repeat ELPs K_2, VK, and V_2, f_e was 0.23 ± 0.06, 0.43 ± 0.10, and 0.57 ± 0.03, respectively. On triple-repeat ELP-modified electrodes with K_3, KVK and VKV, f_e was 0.32 ± 0.03, 0.55 ± 0.09, and 0.77 ± 0.04, respectively. ANOVA and *post hoc* analysis (Tables S3 and S4) indicated that the average hydrophobicity of the guest residues had a significant impact on electron transfer for double- and triple repeat peptide samples.

3.3. A quantitative model for effective surface coverage

To compare the relative mass loading on gold electrodes of different ELPs, hydrated mass loading of ELPs was estimated using a quartz crystal microbalance with dissipation (QCM-D). Table S5 shows estimated relative hydrated mass loadings for all peptides in this study, and Fig. S3 shows representative QCM-D runs of triple-repeat ELPs.

Given that relative mass loading and hydrophobicity were hypothesized to significantly affect the f_e, we proposed the following model:

$$f_e = k_e\, S\, (H) + f_{e,\,min} \quad (2)$$

Where k_e is a parameter to describe the dependence of f_e on hydrophobicity and pentapeptide loading (cm^2 ng^{-1}), S is the mass loading of elastin per unit area (ng cm^{-2}), and $f_{e,min}$ is the minimal amount of coverage for a monolayer of elastin. H is the relative hydrophobicity normalized to valine such that H is the average hydropathy compatibility index of the guest residues divided by the hydropathy compatibility index of valine [24]. Calculation examples are provided in Table S6.

Based on Eq. 2, a plot of f_e versus H*S will yield a straight line, where the slope is equal to k_e and the intercept represents $f_{e,\,min}$. Fig. 3 shows f_e values calculated from data represented in Figs. 1 and 2 plotted as a function of H*S. Linear regression was performed on average values and the linear relationship between f_e and H*S was statistically significant (see Fig. S4, and Table S7 for regression results).

Conditions such as scan rate, redox probe concentration and PBS concentration were varied to identify impact on the model. Experiments conducted at different scan rates are provided in Supplementary Data Fig. S5 and S6. Based on the results, scan rate needs to be sufficiently high for the model to be valid. Redox probe concentration was varied, and data collected on VKV peptide-modified SPEs (Fig. S7). When the redox concentration > 1 mM, peak current is 100X greater or more compared to the control of 0 mM redox probe. Thus, the concentration was sufficiently high in experiments used to develop the model. In addition, Fig. S7B shows that there is a linear relationship between peak current and concentration, indicating that the redox probe concentration does not significantly change the properties of the assembled peptide layer. The effect of higher PBS concentrations on the model is shown in Fig. S8, where 10X PBS results in a linear relationship between f_e and H*S, but the slope is lower (~0.0015). This indicates that the model is valid at higher salt concentrations and sufficiently high scan rates, but

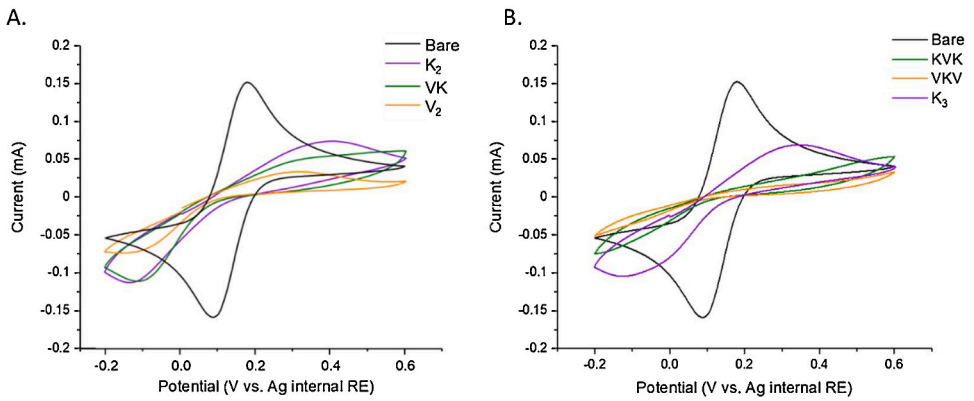

Fig. 2. Cyclic voltammograms demonstrate that the average guest residue hydrophobicity of double- and triple-repeat elastin peptides assembled on gold impact the electron transfer of a label-free redox probe. Results were collected in 0.01 M PBS with 4 mM $Fe(CN)_6^{3-/4-}$ redox couple and 0.1 M KCl, from -0.2 V to 0.6 V (vs. sliver internal reference electrode) with a 0.1 V/s scan rate. Representative cyclic voltammograms are shown for (A) bare electrode (black), K_2 peptide (purple), VK peptide (green), and V_2 peptide (orange); (B) bare electrode (black), K_3 peptide (purple), KVK peptide (green) and VKV peptide (orange).

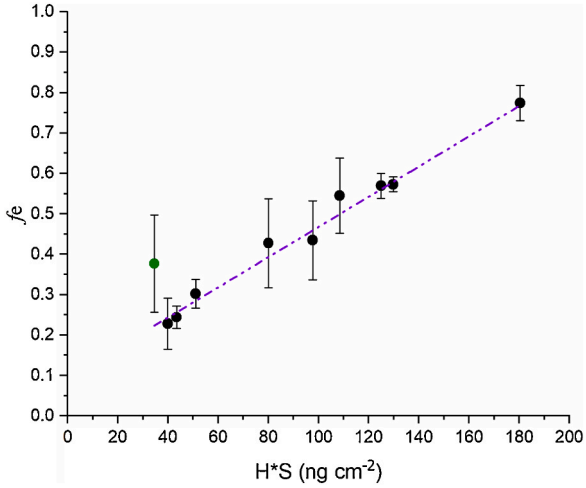

Fig. 3. Effective coverage, *fe*, is linearly related to hydrophobicity compatibility with valine (H) multiplied by the mass loading (S) of ELPs immobilized on gold. Each data point represents the average ± the standard deviation for at least $n = 3$ independent trials. A simple linear regression was performed using Minitab, and the purple line represents the best fit line. Results from the linear regression can be found in the Supplementary Data. The data point in green represents an outlier that is not included in the linear regression for the final model.

the slope may be dependent on ionic strength.

An alternative model based on ELP length instead of mass loading is provided in the Supplementary Data (Fig. S9). In the alternative model, f_e is a linear function of H/L, where each length of peptide has its own distinct slope and L = the number of elastin repeats. As the peptide length increases, the slope increases, indicating the dependence of f_e on H/L becomes stronger such that a small change in hydrophobicity for a long peptide will have a greater impact on f_e. Overall, the alternative model based on length provides additional evidence that f_e may be impacted by the number of hydrophobic interactions in an ELP layer, indicated by the model based on mass loading in Fig. 3 (see Discussion section for more insight into this result).

3.4. The effect of guest residue charge on peptide assembly

The data gathered with the single repeat peptide where X = a negatively charged glutamic acid (E) was higher than expected (shown in green in Fig. 3). Fig. S4 shows that the data point lies outside of the 95 % confidence interval for the linear relationship. Without the outlier, linear regression results in $k_e = 0.0038 \pm 0.0004$ $cm^2\ ng^{-1}$ and $f_{e,min} = 0.093 \pm 0.046$ (95 % confidence intervals). To investigate the electrostatic effect during peptide assembly, we exposed E and K peptides to acidic and basic environments, respectively, to neutralize the guest residues. CV experiments were performed after the assembly in neutralized conditions to quantify the impact on f_e. As demonstrated in Fig. S10, peptides assembled under neutral conditions had the same CV results as when they were assembled in their charged states. This result suggests the electrostatic charge in single-repeat peptides has minimal influence on the peptide assembly on gold. Therefore, further investigation is needed to understand why the outlier exists in our model.

4. Discussion

When considering the physical implications of the model for f_e in Eq. 2, it is important to note that the model (linear fit) was not significant when using the traditional hydrophobicity scales by Wimley and White [25], or the scale developed by Urry based on elastin [26]. The relationship manifested specifically as a function of relative hydrophobe compatibility with valine. Therefore, we speculate that the likely number of hydrophobic interactions, which would be directly related to hydrophobe compatibility with valine (common to all pentapeptide repeats) and the mass loading of the peptides on the surface, is the main predictor of f_e. Similarly, the hydrophobicity of elastin guest residues has been shown to influence mechanical properties [27].

We also note that secondary structure features of the immobilized ELPs may play a role in the observed model, as they change as a function of hydrophobicity. It has been previously demonstrated that guest residue substitutions, specifically hydrophobicity, can alter the propensity of elastin to form α-, β-, and π-turns in solution [28]. In a recent study, β-turn propensity alone was not a significant driver of ELP properties in solution, but when dimerization was considered, the β-turn content altered ELP properties, specifically hydrophobic accessible surface area [29]. The short ELP surface-assembled structures were investigated in our previous work, where Au-binding was shown to only occur when the cysteine moiety was included in the sequence, and the characteristic β-turn structure was observed when the peptides were immobilized to gold [15–17]. In this current study, surface-immobilized triple-repeat ELPs, VKV and KVK, were investigated by atomic force microscopy (AFM), and results are provided in SI (Fig. S11). The AFM reveals that the triple-repeat ELPs have distinct topological features when attached to a gold surface. Circular dichroism (CD) was utilized in our study to qualitatively analyze the characteristic features of triple-repeat ELPs in aqueous condition. The secondary structures were more distinct with the increasing fraction of valine (Fig. S12), indicating the ELP structures in solution are at least correlated with the results in Fig. 3, and surface-bound structure is worthy of future investigation.

The importance of the developed model is that it can be used to predict the effective coverage of different short ELPs when immobilized on surfaces with various combinations of guest residues. We note that while it is somewhat analogous to previous models which predict the transition temperature of higher molecular weight ELPs in solution [7,

30], our model is not describing LCST behavior, but instead the properties which impact the accessibility of the surface to aqueous components. For example, this model can be applied to designing peptide-functionalized surfaces to control electrode organization, where accessibility of the modified electrode surface is desired. We recently published studies where a single-repeat ELP sequence (X = E) enhanced the ionic transport of a thin ionomer layer, despite being adsorbed to the gold electrodes [15]. This current study shows that a single-repeat peptide where X = E would have relatively low f_e, thus corroborating the results of our previous study. Another area where the model will have impact is in the field of sensor design where ELPs are proposed as an active transducer [11]. It would be ideal to have the greatest difference in f_e between ELP in the soluble and insoluble states, and this study provides a basis on which future work optimizing ELP-based sensor sequences can be built. This study also provides direction for future studies where the impact of bound ELP on redox probe diffusion, electrochemically active surface area, and electron transfer rate will be fully elucidated and quantified.

5. Conclusion

This work elucidates the relationship between effective surface coverage, ELP guest residue, and mass loading for ELP sequences immobilized to gold. Specifically, there exists a linear relationship between effective coverage and the product of the ELP guest residue hydrophobe compatibility with valine and mass loading. This model demonstrates the potential for ELPs to be precisely designed for future electrochemical and biomaterial applications.

CRediT authorship contribution statement

Zihang Su: Conceptualization, Methodology, Formal analysis, Investigation, Resources, Data curation, Writing - original draft, Visualization. **ChulOong Kim:** Investigation, Formal analysis, Writing - review & editing. **Julie N. Renner:** Conceptualization, Methodology, Formal analysis, Writing - review & editing, Supervision, Project administration, Funding acquisition.

Declaration of Competing Interest

The authors report no declarations of interest.

Acknowledgements

This work was supported by the United States Department of Agriculture (2018-68011-28691) and the National Science Foundation (1739473). The authors acknowledge Dr. Smarajit Bandyopadhyay for CD assistance, Prof. Chung-Chiun Liu and Dr. Yifan Dai from electronics design center in CWRU for helpful discussions.

Appendix A. Supplementary data

Supplementary material related to this article can be found, in the online version, at doi:https://doi.org/10.1016/j.bej.2021.107933.

References

[1] J.N. Renner, S.D. Minteer, Minireview the Use of Engineered Protein Materials in Electrochemical Devices, 2016, pp. 980–985, https://doi.org/10.1177/1535370216647127.
[2] Q. Liu, J. Wang, B.J. Boyd, Peptide-based biosensors, Talanta 136 (2015) 114–127, https://doi.org/10.1016/j.talanta.2014.12.020.
[3] M. Rasmussen, S.D. Minteer, Biosensors and bioelectronics enzymatic biofuel cells: 30 years of critical advancements, Biosens. Bioelectron. 76 (2016) 91–102, https://doi.org/10.1016/j.bios.2015.06.029.
[4] D.W. Urry, Physical chemistry of biological free energy transduction as demonstrated by elastic protein-based polymer, J. Phys. Chem. B 5647 (1997) 11007–11028, https://doi.org/10.1021/jp972167t.
[5] J. Andrew MacKay, D.J. Callahan, K.N. FitzGerald, A. Chilkoti, Quantitative Model of the Phase Behavior of Recombinant pH-Responsive Elastin-Like Polypeptides, Biomacromolecules . 11 (2010) 2873–2879, https://doi.org/10.1021/bm100571j.
[6] J. Reguera, D.W. Urry, T.M. Parker, D.T. McPherson, J.C. Rodríguez-Cabello, Effect of NaCl on the exothermic and endothermic components of the inverse temperature transition of a model elastin-like polymer, Biomacromolecules 8 (2007) 354–358, https://doi.org/10.1021/bm060936l.
[7] D.E. Meyer, A. Chilkoti, Quantification of the effects of chain length and concentration on the thermal behavior of elastin-like polypeptides, Biomacromolecules 5 (2004) 846–851, https://doi.org/10.1021/bm034215n.
[8] D.W. Urry, C.H. Luan, T.M. Parker, D.C. Gowda, K.U. Prasad, M.C. Reid, A. Safavy, Temperature of polypeptide inverse temperature transition depends on mean residue hydrophobicity, J. Am. Chem. Soc. 113 (1991) 4346–4348, https://doi.org/10.1021/ja00011a057.
[9] A.K. Varanko, J.C. Su, A. Chilkoti, Elastin-like polypeptides for biomedical applications, Annu. Rev. Biomed. Eng. (2020) 343–369, https://doi.org/10.1146/annurev-bioeng-092419-061127.
[10] N. Nath, A. Chilkoti, Creating "smart" surfaces using stimuli responsive polymers, Adv. Mater. 14 (2002) 1243–1247, https://doi.org/10.1002/1521-4095(20020903)14:17<1243::AID-ADMA1243>3.0.CO;2-M.
[11] M.A. Morales, W.A. Paiva, L. Marvin, E.R.M. Balog, J.M. Halpern, Electrochemical characterization of the stimuli-response of surface-immobilized elastin-like polymers, Soft Matter 15 (2019) 9640–9646, https://doi.org/10.1039/c9sm01681c.
[12] C.J. Barile, E.C.M. Tse, Y. Li, T.B. Sobyra, S.C. Zimmerman, A. Hosseini, A. A. Gewirth, Proton switch for modulating oxygen reduction by a copper electrocatalyst embedded in a hybrid bilayer membrane, Nat. Mater. 13 (2014) 619–623, https://doi.org/10.1038/nmat3974.
[13] J. Bao, C. Hou, D. Huo, Q. Dong, X. Ma, X. Sun, M. Yang, K.H.A. El Galil, W. Chen, Y. Lei, Sensitive and selective electrochemical biosensor based on ELP-OPH/BSA/TiO 2 NFs/AuNPs for determination of organophosphate pesticides with p -nitrophenyl substituent, J. Electrochem. Soc. 164 (2017) G17–G22, https://doi.org/10.1149/2.0311702jes.
[14] Y. Lu, H. Ang, Q. Yan, E. Fong, Bioinspired synthesis of hierarchically porous MoO2/Mo2C nanocrystal decorated N-doped carbon foam for lithium-oxygen batteries, Chem. Mater. 28 (2016) 5743–5752, https://doi.org/10.1021/acs.chemmater.6b01966.
[15] Z. Su, S. Kole, L.C. Harden, V.M. Palakkal, C. Kim, G. Nair, C.G. Arges, J.N. Renner, Peptide-modified electrode surfaces for promoting anion exchange ionomer microphase separation and ionic conductivity, ACS Mater. Lett. 1 (2019) 467–475, https://doi.org/10.1021/acsmaterialslett.9b00173.
[16] Z. Su, N. Pramounmat, S.T. Watson, J.N. Renner, Engineered interaction between short elastin-like peptides and perfluorinated sulfonic-acid ionomer, Soft Matter 14 (2018) 3528–3535, https://doi.org/10.1039/c8sm00351c.
[17] N. Pramounmat, C.N. Loney, C. Kim, L. Wiles, K.E. Ayers, A. Kusoglu, J.N. Renner, Controlling the distribution of perfluorinated sulfonic acid ionomer with elastin-like polypeptide, ACS Appl. Mater. Interfaces 11 (2019) 43649–43658, https://doi.org/10.1021/acsami.9b11160.
[18] J.C.M. Van Hest, X. Xu, V. Lemieux, P.H.H.M. Adams, J.C.M. Van Hest, Elastin-based stimuli-responsive gold nanoparticles, Chem. Commun. 46 (2010), https://doi.org/10.1039/b923280j.
[19] H.C. Huang, Y. Yang, A. Nanda, P. Koria, K. Rege, Synergistic administration of photothermal therapy and chemotherapy to cancer cells using polypeptide-based degradable plasmonic matrices, Nanomedicine 6 (2011) 459–473, https://doi.org/10.2217/nnm.10.133.
[20] S. Cheemalapati, M. Ladanov, B. Pang, Y. Yuan, P. Koria, Y. Xia, A. Pyayt, Dynamic visualization of photothermal heating by gold nanocages using thermoresponsive elastin like polypeptides, Nanoscale 8 (2016) 18912–18920, https://doi.org/10.1039/c6nr04676b.
[21] K. Vogele, J. List, G. Pardatscher, N.B. Holland, F.C. Simmel, T. Pirzer, Self-assembled active plasmonic waveguide with a peptide-based thermomechanical switch, ACS Nano 10 (2016) 11377–11384, https://doi.org/10.1021/acsnano.6b06635.
[22] S. Chen, L. Li, C. Zhao, J. Zheng, Surface hydration: principles and applications toward low-fouling/nonfouling biomaterials, Polymer (Guildf). 51 (2010) 5283–5293, https://doi.org/10.1016/j.polymer.2010.08.022.
[23] A.L. Furst, A.C. Hoepker, M.B. Francis, Quantifying hormone disruptors with an engineered bacterial biosensor, ACS Cent. Sci. 3 (2017) 110–116, https://doi.org/10.1021/acscentsci.6b00322.
[24] J.C. Biro, Amino acid size, charge, hydropathy indices and matrices for protein structure analysis, Theor. Biol. Med. Model. 12 (2006) 1–12, https://doi.org/10.1186/1742-4682-3-15.
[25] W.C. Wimley, S.H. White, At membrane interfaces, Nat. Strutural Biol. 3 (1996) 842–848.
[26] D.W. Urry, C.-H. Luan, A New Hydrophobicity Scale and Its Relevance to Protein Folding and Interactions at Interfaces, 1995, pp. 92–110, https://doi.org/10.1021/bk-1995-0602.ch007.
[27] S. Hollingshead, J.C. Liu, pH-sensitive mechanical properties of elastin-based hydrogels, Macromol. Biosci. 20 (2020) 1–12, https://doi.org/10.1002/mabi.201900369.
[28] A. Prhashanna, P.A. Taylor, J. Qin, K.L. Kiick, A. Jayaraman, Effect of peptide sequence on the LCST-like transition of elastin-like peptides and elastin-like peptide-collagen-like peptide conjugates: simulations and experiments,

Biomacromolecules 20 (2019) 1178–1189, https://doi.org/10.1021/acs.biomac.8b01503.

[29] Y. Zhang, V. Zai-Rose, C.J. Price, N.A. Ezzell, G.L. Bidwell, J.J. Correia, N. C. Fitzkee, Modeling the early stages of phase separation in disordered elastin-like proteins, Biophys. J. 114 (2018) 1563–1578, https://doi.org/10.1016/j.bpj.2018.01.045.

[30] A. Ghoorchian, N.B. Holland, Molecular architecture influences the thermally induced aggregation behavior of elastin-like polypeptides, Biomacromolecules 12 (2011) 4022–4029, https://doi.org/10.1021/bm201031m.